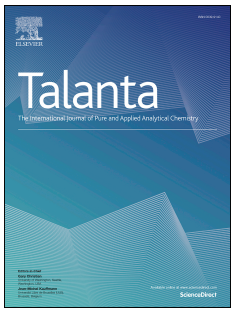

Electrochemical nano-genosensor for highly sensitive detection of miR-21 biomarker based on SWCNT-grafted dendritic Au nanostructure for early detection of prostate cancer

Abbas Sabahi, Razieh Salahandish, Ali Ghaffarinejad, Eskandar Omidinia

PII: S0039-9140(19)31228-7

DOI: https://doi.org/10.1016/j.talanta.2019.120595

Reference: TAL 120595

To appear in: *Talanta*

Received Date: 4 September 2019

Revised Date: 24 November 2019

Accepted Date: 25 November 2019

Please cite this article as: A. Sabahi, R. Salahandish, A. Ghaffarinejad, E. Omidinia, Electrochemical nano-genosensor for highly sensitive detection of miR-21 biomarker based on SWCNT-grafted dendritic Au nanostructure for early detection of prostate cancer, *Talanta* (2019), doi: https://doi.org/10.1016/j.talanta.2019.120595.

Electrochemical nano-genosensor for highly sensitive detection of miR-21 biomarker based on SWCNT-grafted dendritic Au nanostructure for early detection of prostate cancer

Abbas Sabahi[a,b], Razieh Salahandish[a,b], Ali Ghaffarinejad[a,b*], Eskandar Omidinia[c]*

[a] *Research Laboratory of Real Samples Analysis, Faculty of Chemistry, Iran University of Science and Technology (IUST), Tehran 1684613114, Iran*
[b] *Electroanalytical Chemistry Research Center, Iran University of Science and Technology (IUST), Tehran 1684613114*
[c] *Department of Biochemistry, Genetic and Metabolism Research Group, Pasteur Institute of Iran, Tehran 13164*

* Corresponding authors:
Ali Ghaffarinejad:
Email: Ghaffarinejad@iust.ac.ir; Tel: +98-21-77240652; Fax: +98-21-73021554
Eskandar Omidinia:
Email: skandar@pasteur.ac.ir and eomid8@gmail.com; Tel: +98-21-66969298

ABSTRACT

MicroRNAs (miRNAs) appear as a novel reliable candidate in biomarkers for early diagnosis of cancer. Due to their roles in various types of cancer, their potential as a diagnostic biomarker is getting more attention. Here, a novel electrochemical biosensor for detection of miR-21 was demonstrated, through combining the advantages of electrochemical methods and nanomaterials with the selectivity of oligonucleotides, based on thiolated receptor probe-functionalized dendritic gold nanostructures (den-Au) via the self-assembly monolayer (SAM) process which grafted on the single-wall carbon nanotubes (SWCNTs) platform on the surface of the fluorine-doped tin oxide (FTO) electrode. Cadmium ions (Cd^{2+}) were used as signal units and also signal amplification substance which labeled before on miR-21 target. The oxidation signal of Cd^{2+} as a signal unit was measured by differential pulse voltammetry (DPV) technique that had a very wide linear relationship with the concentration of miR-21 target (0.01 fmol L^{-1} to 1 μmol L^{-1}) and low experimental detection limit of 0.01 fmol L^{-1}. Furthermore, fabricated biosensor showed acceptable performance in human serum samples and also good selectivity indiscriminate between the complementary target and non-complementary one, so this nano-genosensor can clinically be used for prostate cancer diagnosis through the detection of miR-21 in human serum samples.

Keywords: MiRNA-21; Electrochemical nano-genosensor; Oligonucleotide; Dendritic gold nanostructures; Single wall carbon nanotubes; Prostate cancer

1. Introduction

Worldwide, cancer is known as one of the main causes of human mortality [1, 2]. Prostate cancer (PCa) is the most common non-skin cancer worldwide also diagnosed male malignancy and is the second leading cause of male cancer-related death worldwide [3, 4]. Diagnosis of prostate cancer is routinely done by using prostate-specific antigen (PSA) test for early detection [5, 6], however, this test has its own limitations including specificity and ambiguity on the optimal threshold for biopsy [7]. Additionally, high levels of PSA are not necessarily related to the cancerous state of prostate and may fluctuate due to the infections, inflammation, or benign prostatic hyperplasia (BPH) thus resulting in misdiagnosis and overtreatment of indolent PCa [8, 9]. Consequently, it is crucial to utilize more effective biomarkers to improve PCa prognosis and diagnosis.

MiRNAs are short, endogenous and non-coding RNAs (~22 nucleotides) found in the diverse organisms and generally play crucial roles in all biological pathways including cell proliferation, differentiation, and apoptosis [10, 11]. They also have the potential of being excellent biomarkers candidate for cancer diagnosis, prognosis, and therapy, as they can be isolated and detected from a wide range of biological samples [12], including blood, urine, saliva, plasma and serum [13]. Studies have indicated a strong correlation between the expression patterns of miRNAs with various types of diseases, including cancer [12, 14], diabetes [15], neurological disorders [16], rheumatic diseases [17], and cardiovascular disorders [18]. Among numerous types of miRNAs, miR-21 has been identified as the only one to be over-expressed in 11 types of cancerous tumors including stomach, prostate, head and neck, pancreas, lung, colorectal, esophagus, glioblastoma, and neuroblastoma [19, 20]. Even though, miRNA's, including miR-21 molecules, show a very strong correlation with various cancers, and are considered to be a

strong contender as a potential prognostic and/or diagnostic biomarker, there are some challenges associated with their detection. Some of the limitations include low levels of expression, highly homologous sequence, small size, and presence of wide range of variants [21, 22]. Many conventional methods currently employed in detection of these molecules are labor intensive, time consuming, low on sensitivity and involves multistep complicated protocols and procedures [23-26]. Considering above mentioned limitations, it is imperative to develop some new highly sensitive and selective assay for detection and quantification of these miRNAs. Some of the most recent methods invented for sensitive detection of miRNAs involve quantification methods are based on fluorescence [27], colorimetry [28], electrochemistry [29], bioluminescence [30], chemiluminescence [31], electrochemiluminescence [32], surface plasmon resonance [33], and capillary electrophoresis assays [34]. Among these methods, electrochemical biosensors have attracted a lot of attention due to it's rapid, sensitive, selective, and cost-effective properties [35]. Electrochemical biosensors based on signal amplification have been investigated to detect miRNAs for enhanced sensitivity, selectivity, and low detection limit [36]. Different types of labels ranging from gold nanoparticles [37], OsO_2 nanoparticles [38], carbon nanotube [39], graphene [40], enzyme [41], triple signal amplification protocol [42], to quantum dots [43] have been used for signal amplification. Many labeled electrochemical miRNA bisensors have been developed to achieve lowest detection limit. Several of these developed miRNA biosensors include use of tagged quantum dots, Cd^{2+}-modified Tip nanoparticles, RuO_2 nanoparticles, OsO_2 nanoparticles, $Ru(PD)_2Cl_2Os$, and $Os(dmpy)_2(IN)Cl^+$ in conjunction with various electrochemical techniques ranging from anodic strip voltammetry to square wave voltammetry (SWV). With the deployment of these novel quantifying techniques investigators were able to detect

presence of miRNA ranging anywhere from 0.32 amol L^{-1} to 2.0 fmol L^{-1} [38, 44-48]. All of these detection methods showed high sensitivity, selectivity and improved efficiency of electrochemical biosensors based on signal amplification strategy.

Herein, we describe a selective and sensitive FTO based biosensor for the detection of miRNA which has been modified with functionalized SWCNTs and dendritic gold nanostructures (den-Au) to attain high conductivity, increased surface area [49, 50]. Furthermore, the functionalized surface provides an exceptional platform for the immobilization of thiol receptor probes [51, 52] .

DPV is a very sensitive electrochemical technique used to assess selectivity and efficiency of an electrochemical biosensor. We choose DPV as a tool to evaluate performance of our fabricated biosensor for the detection of miR-21 amplicons. Our results indicate that Cd^{2+} as a signal amplification unit, significantly improves the detection signal and consequently enhanced low detection limit with a very wide dynamic range for the high sensitivity and selectivity of proposed nano-genosensor.

2. Experimental

2.1. Materials and oligonucleotides

All chemicals including sulfuric acid (H_2SO_4, 98%), hydrochloric acid (HCl, 37%), ethanol (C_2H_5OH, 99%), sodium hydroxide (NaOH), nitric acid (HNO_3, 65%), potassium ferrocyanide ($K_4Fe(CN)_6$), potassium ferricyanide ($K_3Fe(CN)_6$), phosphoric acid (H_3PO_4, 85%), and cadmium chloride ($CdCl_2$) were purchased from Merck & Co (USA). L-Cysteine, 11-mercapto-1-undecanol (MU), SWCNTs ($\geq$ 95%), gold (III) chloride trihydrate ($HAuCl_4.3H_2O$, $\geq$ 99.9%), and phosphate buffered saline (PBS) were brought from Sigma-Aldrich (USA). All the procured

materials were analytical grade and used without any further purification. To minimize nuclease activity, all glassware and sample tubes firstly treated with pure ethanol and rinsed with by ultra-pure DNase/RNase free water followed by autoclaving. All solutions prepared in RNase/DNase free water. All experiments were done at room temperature except experiments related to temperature optimization tests and cadmium labelling. All oligonucleotides were purchased from Panagene Company (Daejeon, Korea). Both thiolated complementary peptide nucleic acid (PNA) of miR-21 as a receptor probe with the sequence of 5′-SH-$(CH2)_6$-$(Lys)_3$-TCAACATCAGTCTGATAAGCTA-3′, and miR-21 with the sequences of 5′-UAGCUUAUCAGACUGAUGUUGA-3′ was used as a target. Also, the selectivity of biosensor was evaluated by using a non-complimentary miRNA with the sequence of 5′-GUAAGGCAUCUGACCGAAGGCA-3′.

2.2. Apparatus and electrochemical measurements

All electrochemical measurements were carried out with Autolab PGSTAT 204N (Potentiostat/Galvanostat; Echo chemie, B. V.) equipped with Nova 1.11 software. The three-electrode model system comprised of a platinum rod as the auxiliary electrode (AE), Ag/AgCl, 3 mol L^{-1} KCl as the reference electrode (RE), and a modified FTO electrode as the working electrode (WE). The electrochemical response of Cd^{2+} oxidation was measured by DPV technique with the potential window of -1.5 V to 0 V and the sweep rate of 100 mV s^{-1} in PBS (pH 7.4). The electrochemical impedance spectroscopy (EIS) was performed within the frequency range of 10 mHz – 100 kHz, with the potential amplitude of 14 mV around the open circuit potential (E_{ocp}). The crystalline structure and morphology were characterized by XRD (Bruker D8 ADVANCE, Cu Kα radiation, λ = 1.5406 nm), field emission scanning electron microscope (FESEM) images and elemental

mapping analysis were taken by Carl Zeiss instrument model MIRA3 and scanning electron microscope (SEM) images with Carl Zeiss model VEGA2, both of them from TESCAN Company.

2.3. Preparation of the nanocomposite

To minimize any contaminations that could affect the electrochemical process, the FTO electrodes (8 Ω resistance and 0.5×0.5 cm^2 surface area) were washed with acetone and 70% ethanol to eliminate any organic contaminants. The whole system was rinsed with deionized (DI) water and dried by using nitrogen gas. Functionalized CNTs have been shown to have much more solubility in aqueous solvents due to the reduction of van der Waals interactions between CNTs due to the incorporation of functionalized groups [53]. Functionalization of 10mg of SWCNTs to incorporate carboxy groups was done by treatment with a mixture of concentrated H_2SO_4/HNO_3 (3:1) with sonication at 70 °C for 4 h. The left over black solid was filtered and rinsed several times by DI water to remove the extra acid and achieve a neutral pH. The functionalized SWCNTs were then dried in the vacuum oven at 70 ºC for 8 h [54]. The obtained product was dispersed in DI water (0.5 mg mL^{-1}) and sonicated for 1 h to achieve the homogeneous SWCNTs suspension. FTO electrodes were then cast coated with 30 μL of SWCNTs suspension.

In the second stage, den-Au nanostructures were synthesized on top of the SWCNTs substrate by chronoamperometry (CA) technique in the aqueous solution containing of 1.0 mmol L^{-1} $HAuCl_4$ and 0.5 mol L^{-1} H_2SO_4 in the presence of 0.1 mmol L^{-1} L-Cysteine at the constant potential of -0.8 V for 1500 s [55, 56].

2.4. Biosensor fabrication

There are different ways to immobilize oligonucleotides onto the surface of the modified electrode, including adsorption [57], covalent binding [58], self-assembled monolayer (SAM) process [59], and immobilization based on electrochemical oxidation of guanine and adenine groups of those molecules [60]. To fabricate the biosensor and to immobilize the bio-receptor, 30 μL of the PNA probe was cast coated onto the modified electrode SWCNTs/den-Au surface. The complementary probe was attached to the electrode surface by formation of Au-S bond between the thiol functional group at 5-end of the probe with den-Au nanostructures, through the SAM process at room temperature overnight [61]. The resulted biosensor was rinsed with 0.02 mol L^{-1} of PBS to remove any non-specific probes. Furthermore, to eliminate any nonspecific binding, the prepared nanocomposite was immersed in 1 mmol L^{-1} MU for 30 min [52].

2.5. Direct labeling of miR-21

Cd^{2+} was used as a label and signal unit for detection of miR-21 through the electrostatic binding between the positive charge of Cd^{2+} and negative charge of miR-21 phosphate backbone. The direct labeling of miR-21 was performed by incubating of Cd^{2+} with miR-21 in PCR tubes (1000 μL). Various gradient concentrations of miR-21 and $CdCl_2$ as the source of Cd^{2+} ion was incubated at 37 °C for 60 min and stored at -18 °C till further use.

2.6. Hybridization of labeled miR-21 with receptor probe

Finally to hybridize labeled miR-21 with the PNA probe, 30 μL of the labeled target was cast coated on the surface of the fabricated sensor (SWCNT/den-Au/Probe/MU) and incubated at 37 °C for a certain time at 85% humidity. The fabricated biosensor was then rinsed by PBS to remove any unlabeled targets which didn’t conjugate properly onto bio-receptor probes.

2.7. Serum sample preparation

Blood samples were collected from a healthy person aged between 25 and 30 years old from the Pasteur Institute of Iran. Serum, from about 10 mL of blood was obtained by deproteinization method involving centrifugation of blood samples at 2000 rpm for 10 min at 4 °C. About 4 mL of serum was extracted from 10 mL of the blood and was stored at -20 °C. The frozen serum was thawed at room temperature before use.

3. Results and discussions

miR-21 has been considered to be one of the essential oncogenic factor that is found to be overexpressed in variety of cancers including PCa [62, 63]. The aim of this study was to design an electrochemical based biosensor capable of quantifying miR-21 and to evaluate its potential to be a biomarker for PCa. **Figure. 1**, represents step by step fabrication process of nano-genosensor for detection of miR-21 as the biomarker of PCa.

Please insert Fig. 1 here.

3.1. Evaluation of the synthesized nanocomposite

Carbon nanotubes are excellent materials for biosensing application because of their unique structural, mechanical, chemical properties along with exceptional electrical, metallic conductivity, and thermal stability [49, 50]. Furthermore, nanotubes are also shown to provide an ideal platform for immobilization of different types of biomolecules. These unique properties put carbon nanotubes in a distinct class of materials thus bridging chemistry and biology together for better

understanding biochemical systems [64]. Inclusion of carbon nanotubes onto the biosensing surfaces imparts vital features which are very crucial for biosensing application. The FESEM image of SWCNT in **Fig. 2A** elucidates how SWCNT contributes towards an increase in surface area and surface roughness for adsorption of the den-Au nanostructures onto the FTO electrode. **Figure 2B** and **Figure 2C** are the FESEM images for the second layer of nanocomposite composed of den-Au nanostructure.

Inclusion of den-Au nanostructures has shown to induce high chemical stability, high conductivity, increase in the effective surface area [65], and augmented immobilization of thiolated complementary probes onto these nanostructures [52]. To gain a better understanding of mechanisms involved in synthesis of den-Au nanostructures, we investigated correlations between den-Au morphology and L-Cysteine molecules present in the solution. At first, by applying a constant potential through the CA technique acting as an applied force, an electron transfer reaction was made to reduce the Au^{3+} ions to Au nucleus form. L-Cysteine molecules which existed in the solution, acted like a gold blocker because this molecule has thiol group for adsorbing the Au nucleus and also has the amine group to create an amide linkage with the carboxylic groups which existed previously on the surface of functionalized SWCNTs of modified electrode. During the time, the thiol groups of L-Cysteine adsorbed the large quantities of Au nucleus and by aggregation of these nucleus gold nanoparticles created. After that, by sticking the large quantities of gold nanoparticles with each other, an initial growth core was created on the thiol group of L-Cysteine molecules, immobilized on SWCNTs surface through an amide linkage. Also, the presence of these molecules induced an isotropic kinetically aggregation for gold nanoparticles that simultaneously formed wire and dendritic nanostructures. Also, about the hydrogen

bubbles which evolved during the electrodeposition process, they acted as a dynamic template to assist the orientation growth of those den-Au nanostructures. The use of den-Au nanostructures is crucial for electrode modification because it provides a suitable platform to stabilize oligonucleotides and facilitates charge transfer between these molecules with electrode surface, due to their high surface area and excellent conductivity. Moreover, the elemental mapping analysis (**Fig. 2D**) and EDS analysis (**Fig. 2E**) revealed different elements and their dispersion in the nanocomposite. Further confirmation of the formation of the den-Au nanostructures, was confirmed by XRD analysis **Fig. 2F**. The XRD pattern of the FTO/SWCNT/den-AuNS electrode surface (**Fig. 2F**) exhibits four main diffraction peaks at 2θ angels of 39.4, 45.6, 65.8, and 78.8 º which are attributed to the (111), (200), (220) and (311) planes of dendrites Au crystals with a symmetric face-centered cubic (fcc) structure, respectively. Also, this diffraction data are in good agreement with the 04-0784 JCPDS card [56, 66].

Please insert Fig. 2 here.

3.2. Electrochemical investigation of the nanocomposite applying EIS and voltammetry techniques

A stepwise fabrication process for the biosensor is shown in **Fig. 3.** The fabricated biosensor was characterized by EIS and DPV techniques. EIS measurement was an effective and sensitive method to characterize the charge transfer resistance (R_{ct}). The semicircle diameter at higher frequencies is related to R_{ct} of $[Fe(CN)_6]^{3-/4-}$ as a redox probe [67]. Comparing the Nyquist plots between the bare FTO (curve a) and composite (curve b) showed that, the minimum resistance of electron transfer is related to the composite because the presence of den-Au in the nanostructures leads to prepare a high surface area and easier charge transfer for redox probe ions.

When the capture probe was loaded on the surface of the nanocomposite, the R_{ct} increased due to the insulating properties of PNA probes (curve c) which showed the existence of an additional layer, and demonstrated that capture probe had been successfully immobilized on the modified electrode. In the next step, by adding MU to block blank spaces of the nanocomposite, R_{ct} significantly increased (curve d) due to the insulating and non-electroactivity properties of MU. Ultimately (curve e), hybridization of miR-21 with the receptor probe that was previously labeled with Cd^{2+} ions, resulted in decrease R_{ct} compared to the previous step because of the presence of Cd^{2+} as the signal unit which improved the electrostatic interaction with $[Fe(CN)_6]^{3-/4-}$ ions and accelerated electron transfer as a conductor metal. EIS and DPV results approve each other, meaning that by changing the R_{ct} the current density changes in the opposite direction, and the fabrication process of this biosensor is successful.

Please insert Fig. 3 here.

3.3. Optimization of the experimental conditions

After characterization and electrochemical analysis of different layers of the fabricated biosensor, several experimental conditions were optimized to improve sensitivity and the performance of the biosensor. There were several parameters that directly affected biosensor performance including receptor probe concentration, hybridization time, temperature, pH, label interaction time, and label concentration.

To optimize the hybridization reaction between receptor probe and its complementary probe, hybridization reactions were performed with a gradient of receptor probe concentrations at 10^{-11}, 10^{-10}, 2×10^{-10}, 10^{-9}, and 10^{-8} mol L^{-1} and miR-21 (10^{-6} mol L^{-1}) previously labeled with Cd^{2+} ions (0.1 mmol L^{-1}). As shown

in **Fig. 4A**, by increasing the concentration of the receptor probe the difference in current density (Δj) increased up to 10^{-9} mol L^{-1}, and hence no significant change was observed because of saturating the electrode surface by enough concentration of probe molecules and more quantities of probes cannot immobilize on the surface, therefore in high concentrations the current density does not change considerably.

Hybridization time was the second parameter to be optimized. This parameter has an important effect on the biosensor efficiency because the high hybridization can improve the sensitivity of the biosensor. During standardization, reactions were subjected to various hybridization time including 15, 30, 60, 120, and 220 min, respectively. According to **Fig. 4B**, the optimal time for complete hybridization between receptor probe and labeled miR-21 was 30 min and in this time the highest current density was achieved, that indicates complete interaction between these two biological molecules. In this step, the same concentration (10^{-6} mol L^{-1}) of miR-21, with the constant concentration of Cd^{2+} (0.1 mmol L^{-1}) were used.

The pH of supporting electrolyte plays an important role in the biosensor activity and strongly influences on the sensing signal. It has been shown that the pH can affect both the structure and the sequences of oligonucleotides. In a high acidic state, oligonucleotides decompose to their components including sugar, phosphate, and bases and weakly acidic media lead to disruption of their sequences. Bases media breakdown the structures of oligonucleotide with affecting the hydrogen bonds between the pair of primes [68]. The biosensor was tested against various pH values of 2, 5, 7.4, 9, and 11 (**Fig. 4C**). The best media for high performance of biosensor was biological pH (7.4). In acidic state and basic media, the current density significantly decreases because of the breakdown of

oligonucleotides structure and release of their Cd^{2+} into the solution. In pH = 5, many labeled miR-21s are destroyed and release their Cd^{2+} ions into the electrolyte and the received signal is only related to the existent ions on the surface of miR-21s. But in pH = 2, the acidic state of supporting electrolyte was very intense, and this condition destroyed all oligonucleotides including PNA probes and miR-21. In pH = 2, the current density significantly increased in comparison with other pH states due to destroying all of the oligonucleotides and even the MU molecules which had insulated the electrode surface and had prepared an excellent surface with high conductivity and enough active surface area of nanocomposite for oxidation of existing cadmium ions (**Fig. 4D**).

To investigate the optimal temperature, the biosensor was tested at various temperatures (28, 35, 45, 55, and 65 °C) and the signal of Cd^{2+} ions was measured. As shown in **Fig. 4E**, the optimum temperature was 28 °C because at higher temperatures denaturing the oligonucleotides structures may occur [69].

The effect of incubation/interaction time between label and miR-21 is highly important and can effect on sensitivity of the biosensor. To optimize this parameter, various incubation times (45, 60, 75, and 90 min) were tested. According to the reported diagram in **Fig. 4F**, the optimum time for better interaction between cadmium ions and miR-21 was obtained as 60 min. Due to the negative charge of oligonucleotides phosphate backbone [70] and also the ability of cadmium ions for binding covalently to (N7) atoms of guanine bases which exist on oligonucleotides structure [71, 72], cadmium ions can bind on miR-21 through the two kinds of bond including electrostatic and covalently. At first, by passing the time, current density increased until 60 min and after that decreased because at first, Cd^{2+} ions had an electrostatic bond with negatively charged of miR-21, and by during the time they made a covalent bond with N7 atoms of guanine bases on

miR-21, which lead to decrease the current density. Since the covalent bond is stronger than the electrostatic bond and cadmium ions could not release to be oxidized on the electrode surface, after passing 60 min, due to the increase of covalent bonds, the current density decreased significantly. Moreover, because of the neutral charge of PNA probes, cadmium ions only were connected to miR-21 and received signals only related to the labeled miR-21 on the biosensor surface. This parameter was optimized using 10^{-6} mol L^{-1} labeled miR-21 by 0.1 mmol L^{-1} of Cd^{2+}. The label concentration was the last parameter which was optimized. For this reason, the function of the biosensor was tested at these concentrations; 0.1, 0.5, and 1 mmol L^{-1} of Cd^{2+} which were incubated on miR-21 (10^{-6} mol L^{-1}) for 60 min under humidity at 37 ºC. As shown in **Fig. 4G** the lowest concentration of Cd^{2+} for detecting of miR-21 was 0.1 mmol L^{-1}. At the concentrations lower than 0.1 mmol L^{-1} of Cd^{2+}, the oxidation signal of Cd^{2+} could not be received, and consequently, the lowest concentration of label was used in all experiments. All of the experiments were performed three times on three electrodes and each of the electrodes was repeated three times.

Please insert Fig. 4 here.

3.4. Investigation of the performance and sensitivity of the biosensor

To evaluate the biosensors performance in the detection of miR-21, different concentrations of the labeled targets, were tested by a sensitive DPV technique. In this study, DPV analysis indicated variation in electrochemical response of Cd^{2+} ions in response to the capture probe elucidating a direct relation to the miR-21 concentration. **Fig. 5** indicates the calibration curve for detection of miR-21 with R^2 = 0.9947, n = 3 repetition, and also RSD ≤ 6 %. The very wide linear range (0.01 fmol L^{-1} –1 μmol L^{-1}) and low experimental detection limit of 0.01 fmol L^{-1}

indicated that this biosensor is comparable with other electrochemical biosensing strategies for miRNAs detection as shown in **Table 1**. Also, the relative standard deviation of the fabricated biosensor, for the same electrode with five measurements and for five different electrodes were ≤ 5% and ≤ 10%, respectively. Therefore, the proposed biosensor showed good repeatability and reproducibility.

Please insert Fig. 5 here.

Table 1. Comparison of different biosensors for the determination of miRNAs.

Target miRNA	Method of signal amplification	Electrode/Electrochemical method	Linear range	Detection limit	References
miR-21	MoS_2/AuNPs/SA-ALP[a]	GCE/DPV	0.1 fmol L^{-1} -0.1 pmol L^{-1}	0.086 fmol L^{-1}	[73]
miR-21	Au@$CoFe_2O_4$/TbGra[b]/rolling circle	GCE/SWV	1fmol L^{-1} -2nmol L^{-1}	0.3 fmol L^{-1}	[74]
miR-21	AuNPs/capture probe/redox cycling	AuE/DPV	1 fmol L^{-1} -100 pmol L^{-1}	0.36 fmol L^{-1}	[75]
miR-21	AuNPs/SA-ALP/redo cycling	AuE/Amp	10 fmol L^{-1} -5 pmol L^{-1}	3 fmol L^{-1}	[42]
miR-21	Hairpin capture probe/targetrecycling/MB[c]	AuE/DPV	0.5 pmol L^{-1} -2000 pmol L^{-1}	56 fmol L^{-1}	[76]
miR-16	CdSeTe/CdS QDs[d]/ LNA-MB[e]	GCE/ASV	10.0 amol L^{-1} - 10.0 pmol L^{-1}	0.32 amol L^{-1}	[44]
miR-21	TiP−Cd^{2+}/ capture probe	GCE/SWV	1.0 amol L^{-1} - 10.0 pmol L^{-1}	0.76 amol L^{-1}	[45]
miR-21	den-AuNS/ capture probe/ Cd^{2+}	FTO/DPV	0.01 fmol L^{-1} - 1 µmol L^{-1}	0. 01 fmol L^{-1}	This work

[a]SA-ALP: Streptavidin-conjugated alkaline phosphatase; [b]Tb-Gra: Redox molecule (Tb) on graphene; [c]MB: Methyl blue; [d]QDs: Quantum dots; [e]LNA-MB: Locked nucleic acid- Molecular beacon; [f]RCA: Rolling circle amplification.

3.5. Evaluation of the selectivity, stability and real sample tests

The selectivity of the biosensor is an important parameter. To evaluate the selectivity of biosensor, 10^{-8} mol L^{-1} of the non-complementary target was used which comparing to the main target, had a different sequence. As shown in **Fig. 6A**, fabricated biosensor has comparable selectivity for the miR-21. Also, the stability of biosensor is another important feature that effects the performance of the biosensor. To evaluate the effects of time on the performance of the biosensor, a thirty-day period was considered, and the biosensor performance was measured in ten days intervals. According to **Fig. 6B**, over time and after 30 days 80% recovery with RSD ≤ 8% was obtained which indicates an acceptable performance and stability.

Please insert Fig. 6 here.

To examine the efficiency of the fabricated biosensor, serum real samples prepared by standard dilution method, three different concentrations (10 nmol L^{-1}, 0.01 nmol L^{-1}, and 10 fmol L^{-1}) of labeled miR-21 was spiked into the human serum samples and then cast coated on the biosensor surface for evaluating the biosensor performance. As shown in **Fig. 7**, all recoveries were between 97% and 107% with RSD ≤ 3% for three individual measurements. This indicates that fabricated biosensor has excellent performance even in human serum as a complex matrix.

Please insert Fig. 7 here.

4. Conclusions

In summary, a novel electrochemical nano-genosensor has been developed for the detection of miR-21 amplicon as an aid for the early detection of prostate cancer. The biosensor comprises a cost effective FTO electrode has shown an excellent

potential to be a commercial product. Surface modifications of FTO were achieved via fabrication of SWCNTs and den-Au nanostructures. These surface functionalization techniques led to enhanced conductivity and an increase in effective the electrochemical surface area. Furthermore, the thiolated captured probes immobilized onto the den-Au nanostructures through the SAM process proved to be a suitable platform for immobilizing oligonucleotides during our investigation. Final studies done with labeled miR-21 and Cd^{2+} ions with concentrations ranging from 0.01 fmol L^{-1} to 1 μmol L^{-1} indicated an excellent reproducibility and repeatability. In conclusion, we propose that the fabricated biosensor could potentially be used in clinical processes as a point-of-care device for early diagnosis of PCa. Furthermore, our investigation also points out its potential vital role as a monitoring tool for the patients undergoing PCa treatment.

Acknowledgment

The authors would like to gratefully acknowledge the support of this project by Institute Pasteur of Iran and excellent cooperation of Research Councils of Iran University of Science and Technology (IUST). We are also immensely grateful to Dr. Raman Koul for the edition of the manuscript.

References

[1] R. Siegel, J. Ma, Z. Zou, A. Jemal, Cancer statistics, 2014, CA: Cancer J. Clin. 64 (2014) 9-29.

[2] M. Azimzadeh, M. Rahaie, N. Nasirizadeh, K. Ashtari, H. Naderi-Manesh, An electrochemical nanobiosensor for plasma miRNA-155, based on graphene oxide and gold nanorod, for early detection of breast cancer, Biosens. Bioelectron. 77 (2016) 99-106.

[3] A. Jemal, R. Siegel, J. Xu, E. Ward, Cancer statistics, 2010, CA: Cancer J. Clin. 60 (2010) 277-300.

[4] J. Ferlay, E. Steliarova-Foucher, J. Lortet-Tieulent, S. Rosso, J.-W.W. Coebergh, H. Comber, D. Forman, F. Bray, Cancer incidence and mortality patterns in Europe: estimates for 40 countries in 2012, Eur. J. Cancer 49 (2013) 1374-1403.

[5] Y. Chen, P.-X. Yuan, A.-J. Wang, X. Luo, Y. Xue, L. Zhang, J.-J. Feng, A novel electrochemical immunosensor for highly sensitive detection of prostate-specific antigen using 3D open-structured PtCu nanoframes for signal amplification, Biosens. Bioelectron. 126 (2019) 187-192.

[6] R. Wang, W.-D. Liu, A.-J. Wang, Y. Xue, L. Wu, J.-J. Feng, A new label-free electrochemical immunosensor based on dendritic core-shell AuPd@ Au nanocrystals for highly sensitive detection of prostate specific antigen, Biosens. Bioelectron. 99 (2018) 458-463.

[7] I.M. Thompson, P.J. Goodman, C.M. Tangen, M.S. Lucia, G.J. Miller, L.G. Ford, M.M. Lieber, R.D. Cespedes, J.N. Atkins, S.M. Lippman, The influence of finasteride on the development of prostate cancer, New Eng. J. Med. 349 (2003) 215-224.

[8] M.A. Dall'Era, M.R. Cooperberg, J.M. Chan, B.J. Davies, P.C. Albertsen, L.H. Klotz, C.A. Warlick, L. Holmberg, D.E. Bailey, M.E. Wallace, Active surveillance for early□stage prostate cancer, Cancer. 112 (2008) 1650-1659.

[9] S. Ciatto, M. Zappa, R. Bonardi, G. Gervasi, Prostate cancer screening: the problem of overdiagnosis and lessons to be learned from breast cancer screening, Eur. J. Cancer. 36 (2000) 1347-1350.

[10] V. Ambros, The functions of animal microRNAs Nature 431: 350–355, Proc. Natl. Acad. Sci. U.S.A. 103 (2004) 3687-3692.

[11] M.D. Jansson, A.H. Lund, MicroRNA and cancer, Mol. Oncol. 6 (2012) 590-610.

[12] L. Fabris, Y. Ceder, A.M. Chinnaiyan, G.W. Jenster, K.D. Sorensen, S. Tomlins, T. Visakorpi, G.A. Calin, The potential of microRNAs as prostate cancer biomarkers, Eur. Urol. 70 (2016) 312-322.

[13] K. Zen, C.Y. Zhang, Circulating microRNAs: a novel class of biomarkers to diagnose and monitor human cancers, Med. Res. Rev. 32 (2012) 326-348.

[14] C. Lawrie, S. Gal, H. Dunlop, B. Pushkaran, A. Liggins, Pulford k, Banham AH, Pezzella F, Boultwood J, wainscoat JS, Hatton CS and Harris AL: Detection of elevated levels of tumour-associated microRNAs in serum of patients with diffuse large B-cell lymphoma, Br. J. Haematol. 141 (2008) 672-675.

[15] L.B. Nielsen, C. Wang, K. Sørensen, C.H. Bang-Berthelsen, L. Hansen, M.-L.M. Andersen, P. Hougaard, A. Juul, C.-Y. Zhang, F. Pociot, Circulating levels of microRNA from children with newly diagnosed type 1 diabetes and healthy controls: evidence that miR-25 associates to residual beta-cell function and glycaemic control during disease progression, Exp. Diabetes. Res. 2012 (2012).

[16] B.H. Miller, C. Wahlestedt, MicroRNA dysregulation in psychiatric disease, Brain Res. 1338 (2010) 89-99.

[17] E. Salehi, R. Eftekhari, M. Oraei, A. Gharib, K. Bidad, MicroRNAs in rheumatoid arthritis, Clin. Rheumatol. 34 (2015) 615-628.

[18] J.K. Edwards, R. Pasqualini, W. Arap, G.A. Calin, MicroRNAs and ultraconserved genes as diagnostic markers and therapeutic targets in cancer and cardiovascular diseases, J. Cardiovasc. Transl. 3 (2010) 271-279.

[19] Z. Lu, M. Liu, V. Stribinskis, C. Klinge, K. Ramos, N. Colburn, Y. Li, MicroRNA-21 promotes cell transformation by targeting the programmed cell death 4 gene, Oncogene 27 (2008) 4373.

[20] P.P. Medina, F.J. Slack, microRNAs and cancer: an overview, Cell. cycle. 7 (2008) 2485-2492.

[21] K.A. Cissell, S. Shrestha, S.K. Deo, MicroRNA detection: challenges for the analytical chemist, ACS. Publications. 2007.

[22] J. Driskell, A. Seto, L. Jones, S. Jokela, R. Dluhy, Y.-P. Zhao, R. Tripp, Rapid microRNA (miRNA) detection and classification via surface-enhanced Raman spectroscopy (SERS), Biosens. Bioelectron. 24 (2008) 917-922.

[23] S.H. Ramkissoon, L.A. Mainwaring, E.M. Sloand, N.S. Young, S. Kajigaya, Nonisotopic detection of microRNA using digoxigenin labeled RNA probes, Mol. Cell. Probe. 20 (2006) 1-4.

[24] K. Lao, N.L. Xu, V. Yeung, C. Chen, K.J. Livak, N.A. Straus, Multiplexing RT-PCR for the detection of multiple miRNA species in small samples, Biochem. Bioph. Res. 343 (2006) 85-89.

[25] J.Q. Yin, R.C. Zhao, K.V. Morris, Profiling microRNA expression with microarrays, Trends. Biotechnol. 26 (2008) 70-76.

[26] E.R. Mardis, The impact of next-generation sequencing technology on genetics, Trends. Genet. 24 (2008) 133-141.

[27] H. Yin, Y. Zhou, C. Chen, L. Zhu, S. Ai, An electrochemical signal ‘off–on’sensing platform for microRNA detection, Analyst. 137 (2012) 1389-1395.

[28] A. Niazi, O.-N. Jorjani, H. Nikbakht, P. Gill, A nanodiagnostic colorimetric assay for 18S rRNA of Leishmania pathogens using nucleic acid sequence-based amplification and gold nanorods, Mol. Diagn. Ther. 17 (2013) 363-370.

[29] T. Wang, E. Viennois, D. Merlin, G. Wang, Microelectrode miRNA sensors enabled by enzymeless electrochemical signal amplification, Anal. Chem. 87 (2015) 8173-8180.

[30] K.A. Cissell, Y. Rahimi, S. Shrestha, E.A. Hunt, S.K. Deo, Bioluminescence-

based detection of microRNA, miR21 in breast cancer cells, Anal. Chem. 80 (2008) 2319-2325.

[31] S. Bi, J. Zhang, S. Hao, C. Ding, S. Zhang, Exponential amplification for chemiluminescence resonance energy transfer detection of microRNA in real samples based on a cross-catalyst strand-displacement network, Anal. Chem. 83 (2011) 3696-3702.

[32] C. Ma, E.S. Yeung, S. Qi, R. Han, Highly sensitive detection of microRNA by chemiluminescence based on enzymatic polymerization, ANAL. Bioanal. Chem. 402 (2012) 2217-2220.

[33] S. Fang, H.J. Lee, A.W. Wark, R.M. Corn, Attomole microarray detection of microRNAs by nanoparticle-amplified SPR imaging measurements of surface polyadenylation reactions, J. AM. CHEM. SOC. 128 (2006) 14044-14046.

[34] N. Khan, J. Cheng, J.P. Pezacki, M.V. Berezovski, Quantitative analysis of microRNA in blood serum with protein-facilitated affinity capillary electrophoresis, Anal. Chem. 83 (2011) 6196-6201.

[35] A. Abi, M. Lin, H. Pei, C. Fan, E.E. Ferapontova, X. Zuo, Electrochemical switching with 3D DNA tetrahedral nanostructures self-assembled at gold electrodes, ACS. Appl. Mater. Inter. 6 (2014) 8928-8931.

[36] T.G. Drummond, M.G. Hill, J.K. Barton, Electrochemical DNA sensors, Nat. Biotechnol. 21 (2003) 1192.

[37] J. Wang, X. Yi, H. Tang, H. Han, M. Wu, F. Zhou, Direct quantification of microRNA at low picomolar level in sera of glioma patients using a competitive hybridization followed by amplified voltammetric detection, Anal. Chem. 84 (2012) 6400-6406.

[38] Z. Gao, Z. Yang, Detection of microRNAs using electrocatalytic nanoparticle tags, Anal. Chem. 78 (2006) 1470-1477.

[39] F. Li, J. Peng, Q. Zheng, X. Guo, H. Tang, S. Yao, Carbon nanotube-polyamidoamine dendrimer hybrid-modified electrodes for highly sensitive electrochemical detection of microRNA24, Anal. Chem. 87 (2015) 4806-4813.

[40] B. Jin, P. Wang, H. Mao, B. Hu, H. Zhang, Z. Cheng, Z. Wu, X. Bian, C. Jia, F. Jing, Multi-nanomaterial electrochemical biosensor based on label-free graphene for detecting cancer biomarkers, Biosens. Bioelectron. 55 (2014) 464-469.

[41] C. Yang, B. Dou, K. Shi, Y. Chai, Y. Xiang, R. Yuan, Multiplexed and amplified electronic sensor for the detection of microRNAs from cancer cells, Anal. Chem. 86 (2014) 11913-11918.

[42] L. Liu, N. Xia, H. Liu, X. Kang, X. Liu, C. Xue, X. He, Highly sensitive and label-free electrochemical detection of microRNAs based on triple signal amplification of multifunctional gold nanoparticles, enzymes and redox-cycling reaction, Biosens. Bioelectron. 53 (2014) 399-405.

[43] W. Zhu, X. Su, X. Gao, Z. Dai, X. Zou, A label-free and PCR-free electrochemical assay for multiplexed microRNA profiles by ligase chain reaction coupling with quantum dots barcodes, Biosens. Bioelectron. 53 (2014) 414-419.

[44] D. Wang, L. Hu, H. Zhou, E. Abdel-Halim, J.-J. Zhu, Molecular beacon structure mediated rolling circle amplification for ultrasensitive electrochemical detection of microRNA based on quantum dots tagging, Electrochem. Commun. 33 (2013) 80-83.

[45] F.-F. Cheng, T.-T. He, H.-T. Miao, J.-J. Shi, L.-P. Jiang, J.-J. Zhu, Electron transfer mediated electrochemical biosensor for microRNAs detection based on metal ion functionalized titanium phosphate nanospheres at attomole level, ACS. Appl. Mater. Inter. 7 (2015) 2979-2985.

[46] Y. Peng, G. Yi, Z. Gao, A highly sensitive microRNA biosensor based on ruthenium oxide nanoparticle-initiated polymerization of aniline, Chem. Commun.

46 (2010) 9131-9133.

[47] Z. Gao, Y.H. Yu, Direct labeling microRNA with an electrocatalytic moiety and its application in ultrasensitive microRNA assays, Biosens. Bioelectron. 22 (2007) 933-940.

[48] Z. Gao, Y.H. Yu, A microRNA biosensor based on direct chemical ligation and electrochemically amplified detection, Sensor. Actuat. B: Chemical. 121 (2007) 552-559.

[49] J. Shen, W. Huang, L. Wu, Y. Hu, M. Ye, Study on amino-functionalized multiwalled carbon nanotubes, Mater. Sci. Eng: A 464 (2007) 151-156.

[50] A. Osorio, I. Silveira, V. Bueno, C. Bergmann, $H_2SO_4/HNO_3/HCl$—functionalization and its effect on dispersion of carbon nanotubes in aqueous media, Appl. Surf. Sci. 255 (2008) 2485-2489.

[51] E. Fortunato, D. Ginley, H. Hosono, D.C. Paine, Transparent conducting oxides for photovoltaics, MRS. Bull. 32 (2007) 242-247.

[52] J. Mandli, H. Mohammadi, A. Amine, Electrochemical DNA sandwich biosensor based on enzyme amplified microRNA-21 detection and gold nanoparticles, Bioelectrochemistry. 116 (2017) 17-23.

[53] K. Balasubramanian, M. Burghard, Chemically functionalized carbon nanotubes, Small. 1 (2005) 180-192.

[54] Y. Tao, Z.-J. Lin, X.-M. Chen, X.-L. Huang, M. Oyama, X. Chen, X.-R. Wang, Functionalized multiwall carbon nanotubes combined with bis (2, 2′-bipyridine)-5-amino-1, 10-phenanthroline ruthenium (II) as an electrochemiluminescence sensor, Sensor. Actuat. B: Chemical. 129 (2008) 758-763.

[55] X. Du, Z. Zhang, Z. Miao, M. Ma, Y. Zhang, C. Zhang, W. Wang, B. Han, Q. Chen, One step electrodeposition of dendritic gold nanostructures on β-

lactoglobulin-functionalized reduced graphene oxide for glucose sensing, Talanta. 144 (2015) 823-829.

[56] T.-H. Lin, C.-W. Lin, H.-H. Liu, J.-T. Sheu, W.-H. Hung, Potential-controlled electrodeposition of gold dendrites in the presence of cysteine, Chem. Commun. 47 (2011) 2044-2046.

[57] R. Sabzi, B. Sehatnia, M. Pournaghi-Azar, M. Hejazi, Electrochemical detection of human papilloma virus (HPV) target DNA using MB on pencil graphite electrode, J. Iran. Chem. Soc. 5 (2008) 476-483.

[58] G.B. Sukhorukov, M.M. Montrel, A.I. Petrov, L.I. Shabarchina, B.I. Sukhorukov, Multilayer films containing immobilized nucleic acids. Their structure and possibilities in biosensor applications, Biosens. Bioelectron. 11 (1996) 913-922.

[59] C.V. Uliana, J.O. Tognolli, H. Yamanaka, Application of factorial design experiments to the development of a disposable amperometric DNA biosensor, Electroanal. 23 (2011) 2607-2615.

[60] A.O. Brett, S. Serrano, The electrochemical oxidation of DNA, J. Braz. Chem. Soc. 6 (1995) 97-100.

[61] L. Tian, K. Qian, J. Qi, Q. Liu, C. Yao, W. Song, Y. Wang, Gold nanoparticles superlattices assembly for electrochemical biosensor detection of microRNA-21, Biosens. Bioelectron. 99 (2018) 564-570.

[62] T. Li, R.-S. Li, Y.-H. Li, S. Zhong, Y.-Y. Chen, C.-M. Zhang, M.-M. Hu, Z.-J. Shen, miR-21 as an independent biochemical recurrence predictor and potential therapeutic target for prostate cancer, J. UROLOGY. 187 (2012) 1466-1472.

[63] M. Folini, P. Gandellini, N. Longoni, V. Profumo, M. Callari, M. Pennati, M. Colecchia, R. Supino, S. Veneroni, R. Salvioni, miR-21: an oncomir on strike in prostate cancer, Mol. Cancer. 9 (2010) 12.

[64] S. Gupta, C. Murthy, C.R. Prabha, Recent advances in carbon nanotube based electrochemical biosensors, INT. J. Biol. Macromol. 108 (2018) 687-703.

[65] F. Li, X. Han, S. Liu, Development of an electrochemical DNA biosensor with a high sensitivity of fM by dendritic gold nanostructure modified electrode, Biosens. Bioelectron. 26 (2011) 2619-2625.

[66] T. Huang, F. Meng, L. Qi, Controlled synthesis of dendritic gold nanostructures assisted by supramolecular complexes of surfactant with cyclodextrin, Langmuir. 26 (2009) 7582-7589.

[67] Z. Zhu, X. Li, Y. Zeng, W. Sun, Ordered mesoporous carbon modified carbon ionic liquid electrode for the electrochemical detection of double-stranded DNA, Biosens. Bioelectron. 25 (2010) 2313-2317.

[68] I. Moret, J.E. Peris, V.M. Guillem, M. Benet, F. Revert, F. Dasí, A. Crespo, S.F. Aliño, Stability of PEI–DNA and DOTAP–DNA complexes: effect of alkaline pH, heparin and serum, J. Control. Release. 76 (2001) 169-181.

[69] D. Incarnato, S. Oliviero, The RNA epistructurome: uncovering RNA function by studying structure and post-transcriptional modifications, Trends. Biotechnol. 35 (2017) 318-333.

[70] P. Jolly, M.R. Batistuti, A. Miodek, P. Zhurauski, M. Mulato, M.A. Lindsay, P. Estrela, Highly sensitive dual mode electrochemical platform for microRNA detection, Rep-UK. 6 (2016) 36719.

[71] F. Leonarski, L. D'Ascenzo, P. Auffinger, Binding of metals to purine N7 nitrogen atoms and implications for nucleic acids: A CSD survey, Inorg. Chim. Acta. 452 (2016) 82-89.

[72] R.K. Sigel, M. Skilandat, A. Sigel, B.P. Operschall, H. Sigel, Complex formation of cadmium with sugar residues, nucleobases, phosphates, nucleotides, and nucleic acids, Cadmium: From Toxicity to Essentiality, Springer. 2013, pp.

191-274.

[73] H.-L. Shuai, K.-J. Huang, Y.-X. Chen, L.-X. Fang, M.-P. Jia, Au nanoparticles/hollow molybdenum disulfide microcubes based biosensor for microRNA-21 detection coupled with duplex-specific nuclease and enzyme signal amplification, Biosens. Bioelectron. 89 (2017) 989-997.

[74] N. Yu, Z. Wang, C. Wang, J. Han, H. Bu, Combining padlock exponential rolling circle amplification with CoFe2O4 magnetic nanoparticles for microRNA detection by nanoelectrocatalysis without a substrate, Anal. Chim. Acta. 962 (2017) 24-31.

[75] P. Li, Y. Li, Z.K. Zhou, S. Tang, X.F. Yu, S. Xiao, Z. Wu, Q. Xiao, Y. Zhao, H. Wang, Evaporative Self□Assembly of Gold Nanorods into Macroscopic 3D Plasmonic Superlattice Arrays, Adv. Mater. 28 (2016) 2511-2517.

[76] L. Zhou, J. Wang, Z. Chen, J. Li, T. Wang, Z. Zhang, G. Xie, A universal electrochemical biosensor for the highly sensitive determination of microRNAs based on isothermal target recycling amplification and a DNA signal transducer triggered reaction, Microchim. Acta. 184 (2017) 1305-1313.

Figures Captions

Fig. 1. The schematic of various steps of nanocomposite fabrication: (1) Cast coating of functionalized SWCNTs on the surface of FTO electrode; (2) Electrodeposition of den-Au on the SWCNTs substrate; (3) Adsorption of PNA probe through the SAM process on nanocomposite surface; (4) Adding MU for blocking all the blanked spaces and orienting the bonded miR-21 receptor probes; (5) Biological capturing labeled miR-21 through bio-receptors; (6) Electrochemical sensing process for detection of miR-21 by employing DPV.

Fig. 2. The FESEM micrographs of (A) the SWCNT, (B) the den-Au nanostructures, (C) the SEM micrograph of den-Au nanostructures, and (D) the mapping analysis of the SWCNT/den-Au nanostructures, (E) the EDS spectrum of SWCNT/den-Au nanostructures, and (F) XRD pattern of FTO/SWCNT/den-AuNS.

Fig. 3. Electrochemical characterization tests; (A) Nyquist plots, and (B) DPV curves for (a) bare FTO, (b) nanocomposite, (c) nanocomposite/probe, (d) nanocomposite/ probe/MU, and (e) nanocomposite/probe/MU/Cd^{2+} labeled miR-21 as different stages of the electrode fabrication to detect of miR-21 in 0.02 M of PBS containing 2.5 mmol L^{-1} $K_3Fe(CN)_6$ + 2.5 mmol L^{-1} $K_4Fe(CN)_6$.

Fig. 4. Optimization experimental conditions of modified biosensor; (A) Probe concentration; (B) Hybridization time; (C) pH; (D) pH voltammograms; (E) Temperature; (F) Interaction time between label and miR-21; and (G) Label concentration (n=3).

Fig. 5. The electrochemical DPV response for oxidation of 0.1 mmol L^{-1} Cd^{+2}

labeled miR-21 based SWCNTs/den-Au modified electrode; inset: Calibration curve for different concentrations of miR-21.

Fig. 6. (A) The selectivity of the fabricated biosensor for the miR-21 target; (B) The biosensor stability (n = 3).

Fig. 7. Comparison of the biosensor performance for determination of miR-21 in the human serum sample and PBS sample (n=3).

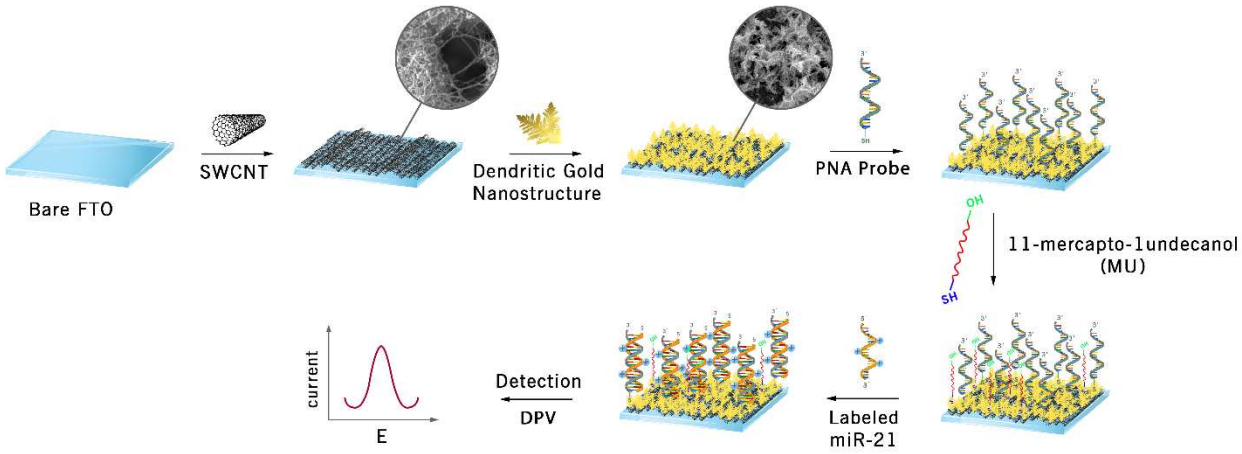

Fig. 1

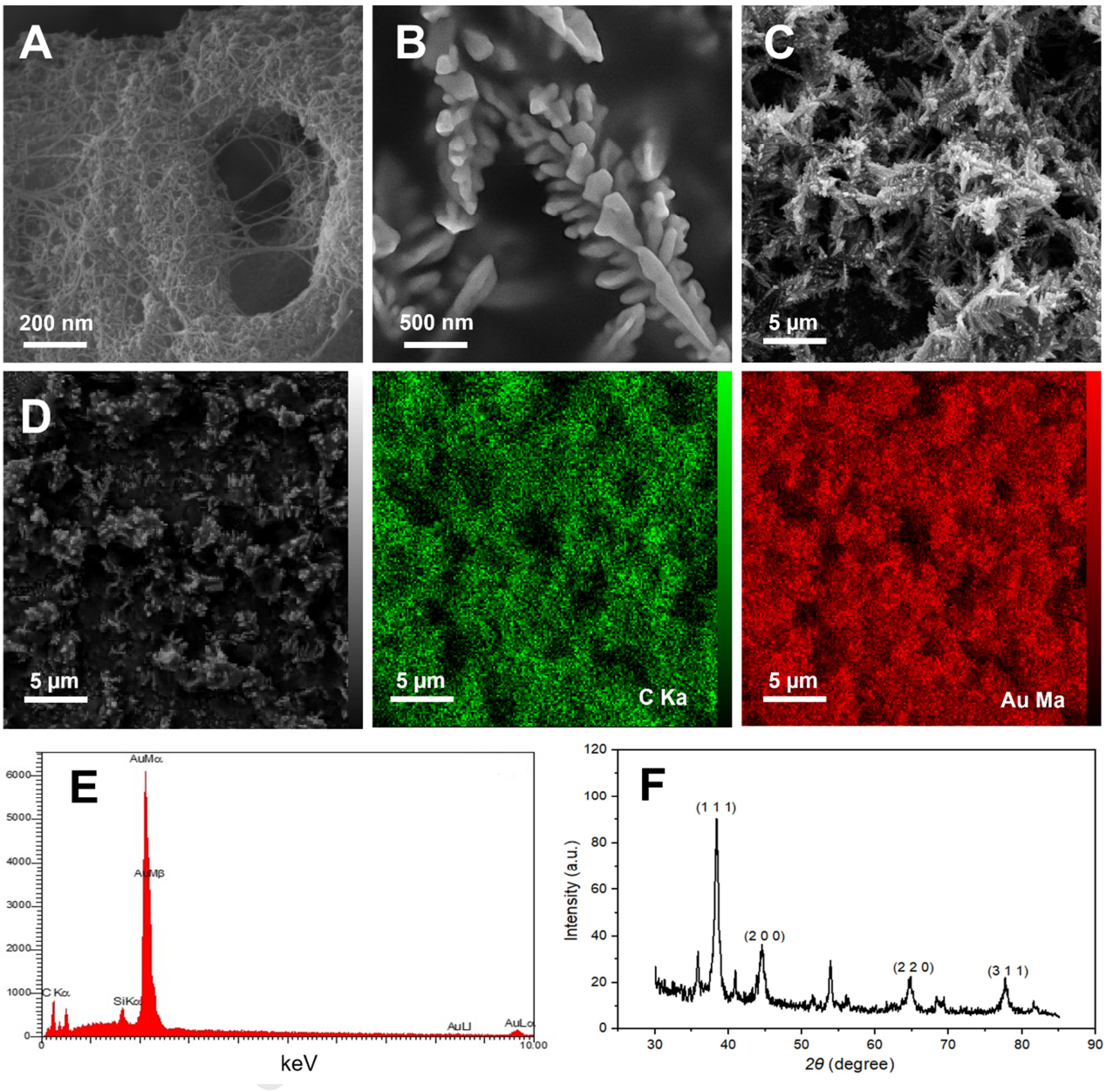

Fig. 2

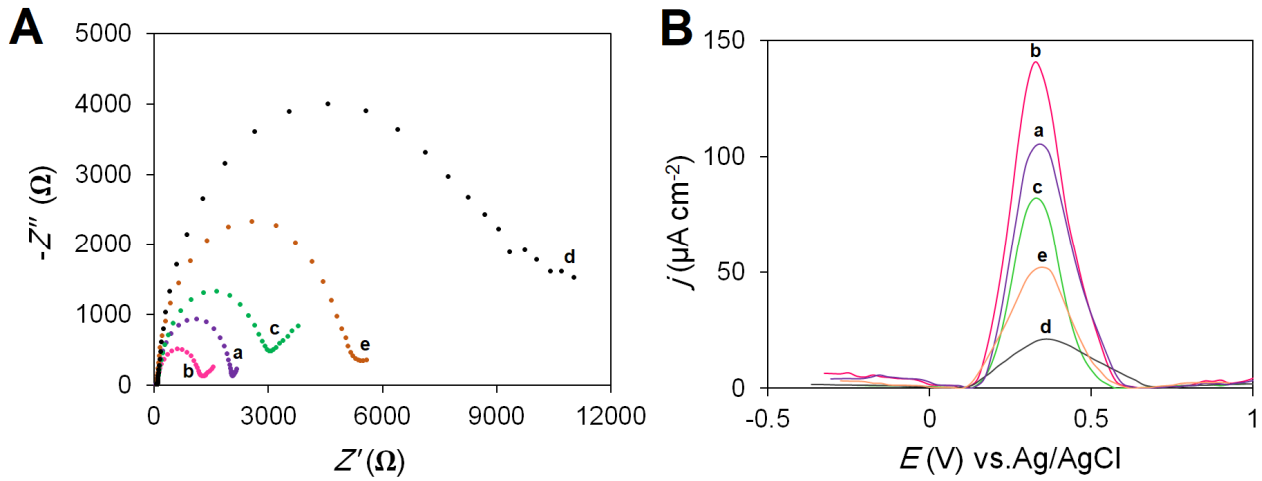

Fig. 3

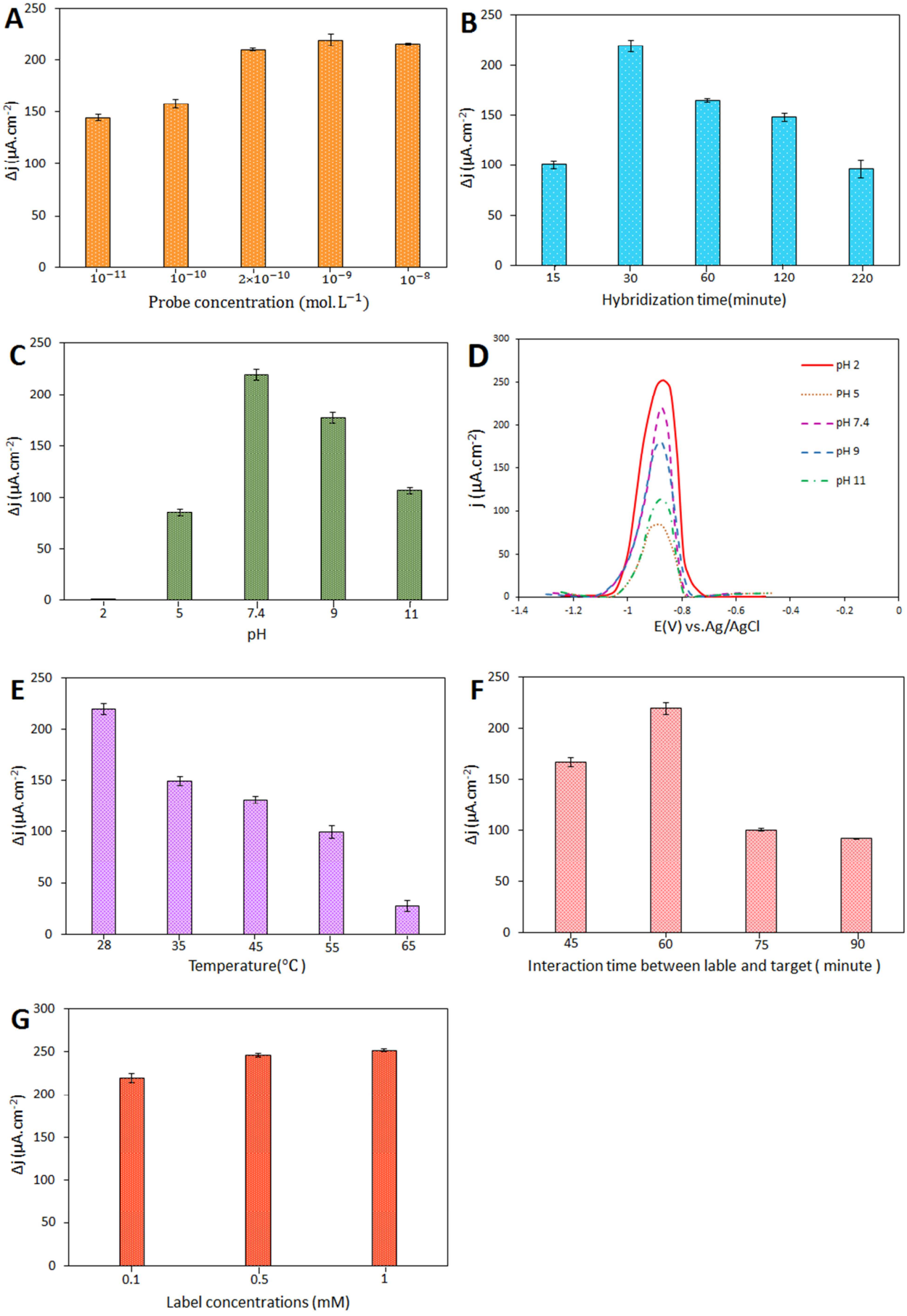
A
Δj (μA.cm⁻²)
Probe concentration (mol.L⁻¹)
10⁻¹¹
10⁻¹⁰
2×10⁻¹⁰
10⁻⁹
10⁻⁸
B
Δj (μA.cm⁻²)
Hybridization time(minute)
15
30
60
120
220
C
Δj (μA.cm⁻²)
pH
2
5
7.4
9
11
D
j (μA.cm⁻²)
E(V) vs.Ag/AgCl
pH 2
pH 5
pH 7.4
pH 9
pH 11
E
Δj (μA.cm⁻²)
Temperature(°C)
28
35
45
55
65
F
Δj (μA.cm⁻²)
Interaction time between lable and target (minute)
45
60
75
90
G
Δj (μA.cm⁻²)
Label concentrations (mM)
0.1
0.5
1

Fig. 4

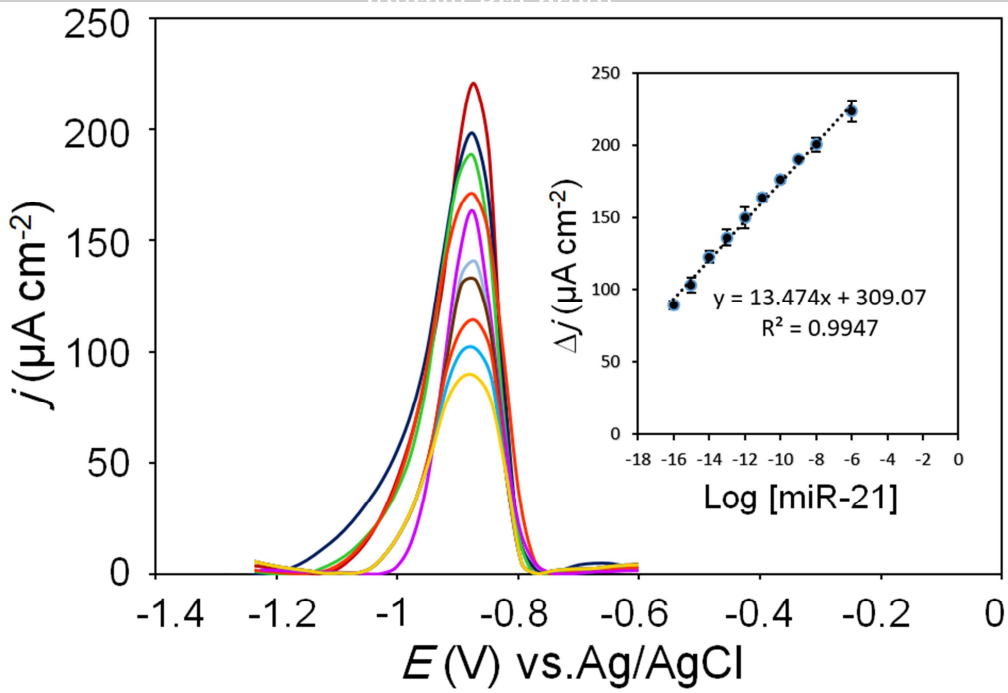

Fig. 5

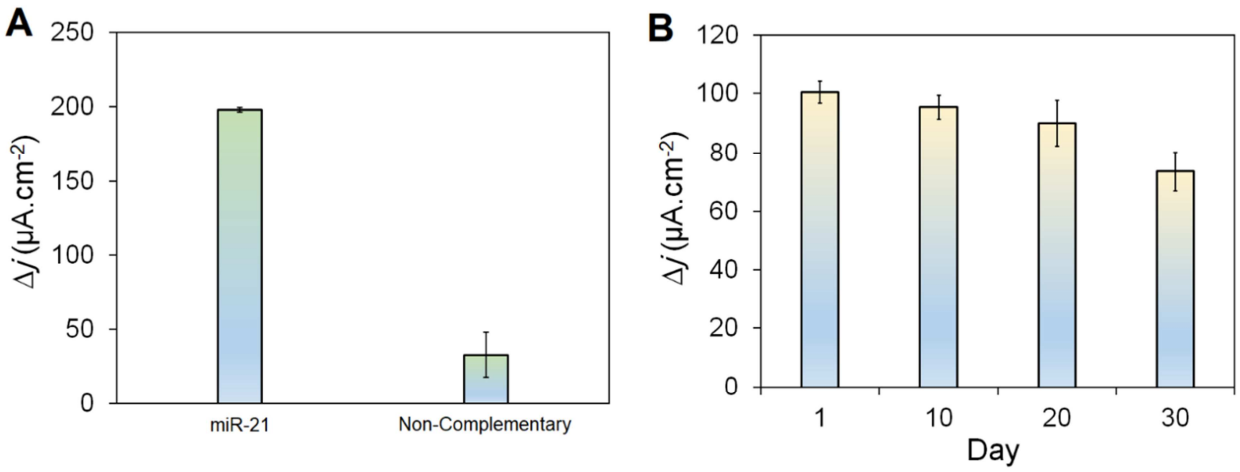

Fig. 6

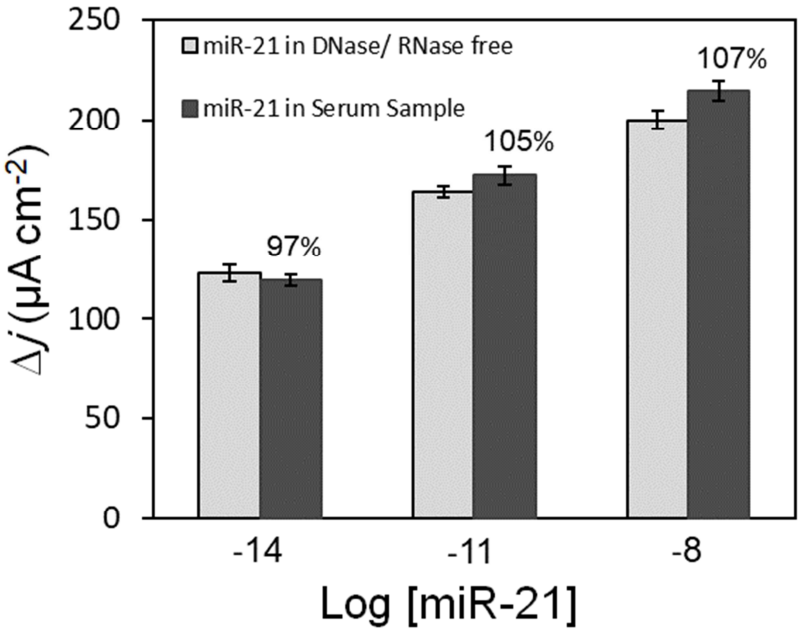

Fig. 7

Highlights

- A new nano-genesensor was introduced for early diagnosis of prostate cancer.
- miR-21 as a biomarker of prostate cancer was measured.
- The nano-genosensor shows high recovery and very wide linear range.
- The biosensor was successfully applied in human serum sample.

Declaration of interests

☒ The authors declare that they have no known competing financial interests or personal relationships that could have appeared to influence the work reported in this paper.

☐The authors declare the following financial interests/personal relationships which may be considered as potential competing interests: